电迁移促进 Cu/Sn-58Bi/Cu焊点阳极界面 Bi层形成的机理分析

何洪文[1,2], 徐广臣[1], 郭 福[1]
(1. 北京工业大学 材料科学与工程学院, 北京 100124; 2. 清华大学 机械工程系, 北京 100084)

摘 要: 研究了 Cu/Sn-58Bi/Cu对接接头焊点在电流密度为 5×10^3 ~ 1.2×10^4 A/cm^2 条件下钎料基体中阳极界面 Bi层的形成机理. 电迁移过程中, Bi元素为主要的扩散迁移元素, 在电迁移力的作用下由阴极向阳极进行迁移. 由于 Bi原子的扩散迁移速度比 Sn原子要快, 促使 Bi原子首先到达阳极界面. 大量的 Bi原子聚集在阳极界面时, 形成了压应力, 迫使 Sn原子向阴极进行迁移, 于是在阳极界面处形成了连续的 Bi层. 阴极处由于金属原子的离去, 形成了拉应力, 导致了空洞和裂纹在界面处的形成. Bi层的形态主要分为平坦的 Bi层和带有凹槽的 Bi层. Bi原子进行扩散迁移的通道有三种: Bi晶界、Sn晶界和 Sn/Bi界面. 随着电流密度和通电时间的增加, Bi层的厚度逐渐增加. 电迁移力和焦耳热的产生成为 Bi原子扩散迁移的主要驱动力.

关键词: 电迁移; Bi层; 电流密度; 焦耳热
中图分类号: TG115 文献标识码: A 文章编号: 0253-360X(2010)10-0035-04

何洪文

0 序 言

电子产品的微型化和智能化促使电子封装中的焊点尺寸持续减小, 使得流经焊点的电流密度会越来越高, 导致电迁移可靠性问题日渐突出[1,2]. 所谓电迁移是指金属原子在高电流密度作用下沿电子运动的方向进行扩散迁移的一种物理现象. 高速运动的电子流形成的电子风与金属原子发生剧烈碰撞, 进行部分的动量交换, 迫使原子沿着电子流方向运动. 电迁移的发生可使得阴极因原子的迁出而产生微空洞或裂纹, 进而减小了流通面积, 电流密度提高, 可能导致断路; 阳极则因原子的迁入而形成凸起的"小丘", 可引发焊点的短路[3,4]. 从本质上讲, 电迁移与其它扩散过程是完全相同的. 各种扩散现象的区别仅在于导致扩散发生的驱动力的不同. 在晶体内、晶界上以及晶体表面上发生的电迁移, 是分别通过晶格扩散、晶界扩散以及晶体表面扩散来完成的[5].

SnBi无铅钎料以其低熔点、低线膨胀系数、高性能, 良好的环境协调性等优点, 被认为是最有希望替代 SnPb钎料的产品之一[6]. 然而, 由于 Bi元素本身的脆性, 过量的 Bi原子聚集会对 SnBi焊点的力学性能产生不良影响, 降低其抗拉强度和塑性. 电迁移过程中, 由于 Bi原子的扩散迁移, 容易在焊点的阳极界面聚集, 从而形成 Bi层或 Bi原子的小丘凸起, 降低焊点的可靠性. 文中主要研究了电流密度为 5×10^3, 1×10^4 和 1.2×10^4 A/cm^2 条件下 Cu/Sn-58Bi/Cu焊点电迁移过程中阳极界面 Bi层形成的机理.

1 试验方法

试验过程中采用 Cu/Sn-58Bi/Cu对接接头, 制备过程主要分为 5个步骤: Sn-58Bi合金的熔炼、焊球的制备、接头的焊接、镶嵌和抛光. 使用纯度均为 99.9% Sn颗粒和 Bi颗粒作为熔炼合金的原材料. 钎料熔炼过程中为了防止氧化, 采用熔盐保护的方法, 熔盐 KCl与 LiCl的质量比为 1.3∶1. 首先, 按 Sn-58Bi的共晶成分称量 Sn粒和 Bi粒的质量, 分别放于清洗干净的坩埚中. 然后使熔盐在 450 ℃时充分熔化, 将液态熔盐覆盖于坩埚中的 Sn粒表面, 再将坩埚放入炉中加热, 温度控制在 500~550 ℃. 待 Sn粒完全熔化后, 将 Bi粒迅速倒入 Sn粒中, 并辅以玻璃棒将其压入保护熔盐下方. 持续保温 40 min, 并每隔 10 min搅拌一次, 以使溶质金属充分溶

收稿日期: 2009-06-16
基金项目: 教育部新世纪优秀人才支持计划资助项目(04-0202)

解. 最后将坩埚取出, 空冷后洗掉熔盐, 放在 350 ℃炉中重熔, 待钎料熔化后, 用玻璃棒搅拌均匀, 迅速将熔化的钎料浇于模具中成形, 制得 Sn-58 Bi(质量分数, %)合金铸锭.

利用射流断裂法将熔炼好的合金铸锭制备成直径约为 300 μm的钎料球, 选用直径为 500 μm的铜线作为连接材料, 在自主设计构建的焊接平台上进行焊接. 具体的焊接步骤参阅文献[7, 8]. 采用冷镶的办法进行试样镶嵌, 镶嵌后首先机械打磨, 然后手工打磨、抛光. 试验前后应用光学显微镜(OM)、扫描电镜(SEM)、能谱分析仪(EDS)观察焊点的微观组织形貌变化. 将抛光好的试样和 DH1718E-5 型双路跟踪稳压稳流电源连通, 电流密度分别为 5×10^3, 1×10^4 和 1.2×10^4 A/cm^2. 试验过程中, 应用热电偶测量并记录焊点的温度, 图 1为电迁移试验的示意图.

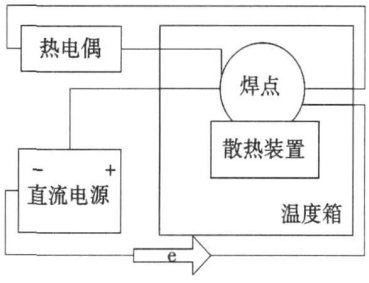

图 1 电迁移试验的示意图

Fig. 1 Schematic drawing of electromigration test

2 试验结果与分析

由于 Sn元素和 Bi元素不发生反应, 而且几乎不固溶, 形成了独特的 Sn-Bi共晶组织. 图 2为典型的 Cu/Sn-58 Bi/Cu焊点的 SEM微观组织形貌: Sn, Bi两相呈均匀分布, 其中颜色高亮的部分为 Bi相, 而颜色较暗的部分为 Sn相, 如图 2箭头所示.

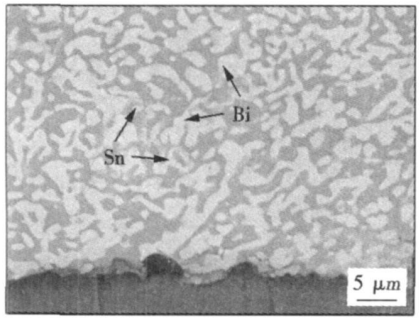

图 2 通电前 Cu/Sn-58 Bi/Cu焊点的微观显微组织

Fig. 2 Microstructure of Cu/Sn-58 Bi/Cu solder joint before current stressing

图 3为 Cu/Sn-58 Bi/Cu焊点在电流密度为 5×10^3 A/cm^2 和环境温度为 80 ℃条件下分别通电 540, 630和 720 h后阳极界面的微观组织形貌的演变, 其中, 图 3d为图 3c的放大像. 采用扫描电镜中的背散射技术, 可以更加清晰的分辨出 Bi相. 通电

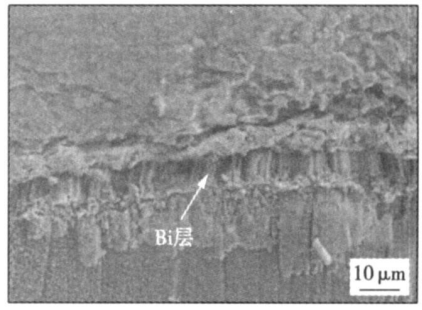

(a) 通电540 h

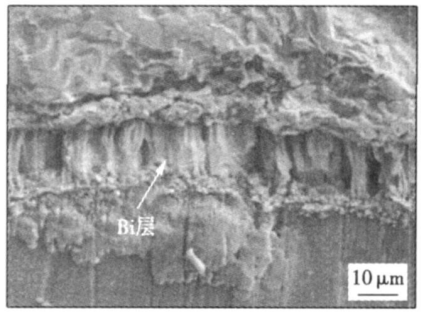

(b) 通电630 h

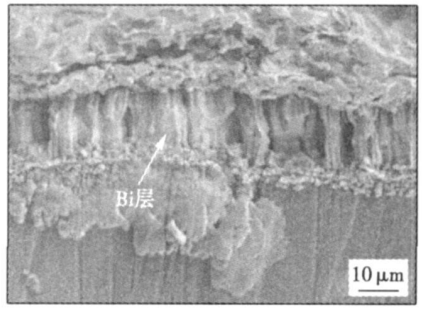

(c) 通电720 h

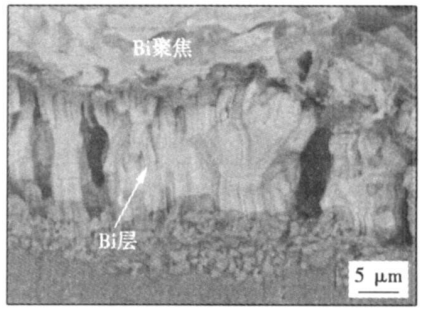

(d) 图3c的放大形貌

图 3 Cu/Sn-58 Bi/Cu焊点在电流密度为 5×10^3 A/cm^2, 80 ℃条件下通电后阳极界面的微观显微组织

Fig. 3 Microstructure of anode interface of Cu/Sn-58 Bi/Cu solder joint at 80 ℃ and current density of 5×10^3 A/cm^2

时间达到 540 h后，在焊点的阳极界面处形成了 Bi层，厚度约为 6.5 μm. 在 Bi层的一侧靠近钎料基体的区域形成了 Bi原子的聚集，而在 Bi层的另一侧靠近铜基板的区域形成了颗粒状的 Cu_6Sn_5 金属间化合物，而且在铜基板上形成了很厚的片状的 Cu_6Sn_5 金属间化合物. Bi层的结构并非很致密，表面凹凸不平. 相对整个基体平面而言，Bi层向里面凹陷，像是镶嵌在基体里面. 表面有很多条纹出现，而且条纹的方向和电子运动的方向平行. 值得一提的是在 Bi层的内部出现了许多的凹槽. 随着通电时间的延长，Bi层的厚度增加. 当通电时间达到 630和 720 h时，Bi层厚度依次为 14.5和 17.5 μm，如图 4所示，为 Bi层厚度的增长曲线. Bi层形成的开始阶段，其厚度增长的较快，通电时间为 630 h时厚度已经达到 14.5 μm，增加了 8 μm；而随着通电时间的继续增加，当到达 720 h时，厚度为 17.5 μm，仅增加了 3 μm. 由此可见，随着通电时间的延长，虽然 Bi层的厚度继续增长，但是增长的速度却变得缓慢.

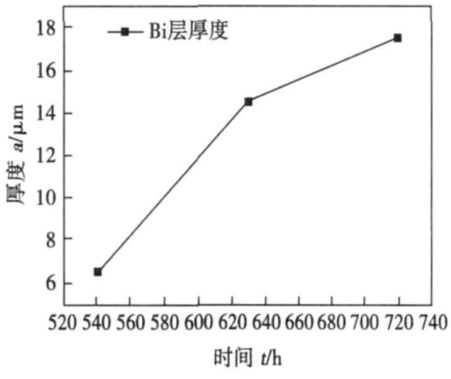

图 4　阳极界面处 Bi层的厚度

Fig. 4　Thickness of Bi layer at anode interface

图 5为 Cu/Sn-58Bi/Cu焊点在电流密度为 1×10^4 A/cm² 室温条件下通电 92 h的微观组织形貌，其中图 5(a)为焊点的阳极界面形貌，图 5(b)为焊点的阴极界面形貌. 图 5(a)中可以观察到，在焊点的阳极界面处 IMC/钎料基体之间形成了连续的 Bi层，厚度约为 10.0 μm. Bi层的表面非常的光滑平整，并未出现凹凸不平和凹槽的形成. 在 Bi层和钎料基体的界面处形成了许多的裂纹. 而且，在 Bi层与铜基板之间同样形成了连续的 Cu_6Sn_5 金属间化合物，而钎料基体仍保持 Sn/Bi的均匀组织，Bi相已粗化长大. 在焊点的阴极附近，出现了不太明显的 Sn聚集. 而且，在钎料 /Cu的界面处形成大量的裂纹和空洞.

图 6所示为 Cu/Sn-58Bi/Cu焊点在电流密度为

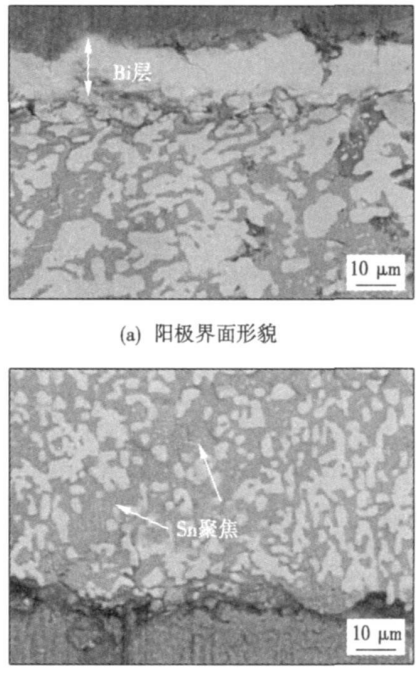

(a) 阳极界面形貌

(b) 阴极界面形貌

图 5　Cu/Sn-58Bi/Cu 焊点在电流密度为 1×10^4 A/cm² 通电 92 h 的微观组织

Fig. 5　Microstructure of Cu/Sn-58Bi/Cu solder joint with current density of 1×10^4 A/cm² after current stressing for 92 h

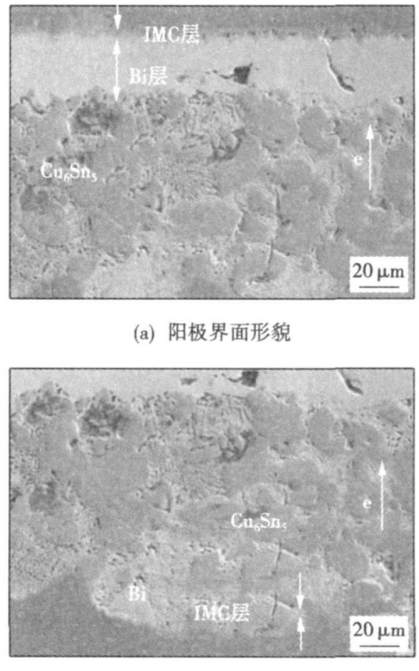

(a) 阳极界面形貌

(b) 阴极界面形貌

图 6　Cu/Sn-58Bi/Cu 焊点在电流密度为 1.2×10^4 A/cm² 通电 80 h 后的微观组织

Fig. 6　Microstructure of Cu/Sn-58Bi/Cu solder joint with current density of 1.2×10^4 A/cm² after current stressing for 80 h

1.2×10^4 A/cm² 下通电时间 80 h后的微观组织形貌，其中图 6a为焊点的阳极局部区域，图 6b为焊点的阴极局部区域．钎料基体中形成了大量的块状的 Cu_6Sn_5 金属间化合物．在这些 Cu_6Sn_5 中间还夹杂着些许 SnBi组织．阳极界面的层状 IMC已经粗化长大，而且厚度非常均匀，约 5.6 μm．在 IMC层和块状 Cu_6Sn_5 之间形成了厚度约为 42.6 μm的 Bi层．焊点的阴极界面由于 Cu原子的熔解扩散已经变得凹凸不平，界面的 IMC厚度很薄，约为 3.8 μm，而且厚度不均匀．

以上试验结果表明，随着通电时间的延长，阳极界面 Bi层的厚度增加．而且，Bi层的厚度和电流密度的大小有关系．当电流密度为 5×10^3 A/cm²，通电时间达到 540 h时，Bi层的厚度仅为 6.5 μm；当电流密度增加至 1×10^4 A/cm² 后，通电仅 92 h，Bi层的厚度就达到了 10.0 μm；而电流密度增加到 1.2×10^4 A/cm² 后，通电 80 h，Bi层的厚度为 42.6 μm，而且钎料基体中形成了大量的 Cu_6Sn_5 金属间化合物．大量焦耳热的形成和电迁移力导致 Cu原子由焊点的阴极向阳极进行扩散迁移．如图 6b所示，焊点的阴极界面已经变得凹凸不平，说明 Cu基板中的 Cu原子向钎料中进行了扩散迁移，和基体中的 Sn原子反应生成了大量的 Cu_6Sn_5 金属间化合物．

Bi原子连续不断的阳极聚集和 Sn原子不断的向反向迁移给 Bi原子的到来腾出足够的空间．当 Bi原子开始向阳极扩散迁移后，由于多余原子的到来在阳极界面附近产生了压应力．而在焊点的阴极，由于原子的离开而产生了拉应力[9]．于是，在整个焊点中产生了应力梯度，梯度的方向是由阴极指向阳极．为了消除这种应力梯度，Sn原子会离开阳极而向阴极进行扩散迁移．所以，通电时间的延长，使得 Bi原子的这种迁移在阳极处不断聚集，从而形成 Bi层．当过量的 Bi原子迁移到阳极时，或者 Sn原子来不及给 Bi原子腾出空间，那么 Bi原子就会在压应力的促使下被挤出界面，形成小丘的堆积．由于 Bi元素的脆性和较高的电阻，Bi层在阳极界面的形成大大降低了焊点的界面强度，导致了更多的焦耳热形成．焦耳热的形成更加促进了 Bi原子的扩散迁移．Bi原子进行扩散迁移的通道有 3种：Bi晶界、Sn晶界和 Sn/Bi界面，如图 7所示．

当 Bi层在阳极界面形成后，几乎所有的 Sn原子已经被排除在 Bi层之外了，根据 Sn-Bi二元相图可知，Sn和 Bi几乎不固溶．Bi层的增长速度可表示[10]为

$$(C_2-C_1)\frac{dy}{dt}=J_{Bi}=C_{Bi}\times\frac{D_{Bi}\times Z^*}{kT}\times e\times\rho\times j$$

式中：y为 Bi层的厚度；t为通电时间；C_1为 Sn在 Bi层中的浓度；C_2为 Sn在钎料基体中的浓度；J_{Bi}为电迁移引发的 Bi的扩散量；C_{Bi}、D_{Bi}和 Z^*分别为 Bi在共晶钎料中的浓度、扩散率和有效电荷数；ρ为共晶 SnBi钎料的电阻率；k为波耳兹曼常数；T为温度；e为电子电荷；j为电流密度．

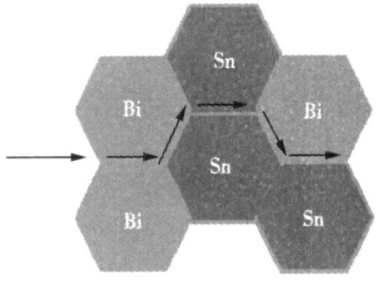

图 7 Bi原子进行扩散迁移的示意图

Fig. 7 Schematic drawing of diffusion and migration of Bi atoms

3 结 论

（1）电迁移过程中，在焊点的阳极界面形成了两种形态的 Bi层：平坦的 Bi层和带有凹槽的 Bi层．随着通电时间的延长，Bi层的厚度增加，但是增长的速度变缓．

（2）电流密度增加，阳极界面的 Bi层厚度增加．Bi层与钎料基体间出现了很多裂纹．而且，当电流密度为 1.2×10^4 A/cm²，通电 80 h时，钎料基体中形成了大量的块状的 Cu_6Sn_5 金属间化合物．

（3）电迁移力和焦耳热的产生成为 Bi原子进行扩散迁移的主要驱动力，方向由阴极指向阳极．Bi原子沿着 Bi晶界、Sn晶界和 Sn/Bi界面进行迁移扩散．

参考文献：

[1] Xu L H, Pang J H L. Combined thermal and electromigration exposure effect on SnAgCu BGA solder joint reliability[C] // Electronic Components and Technology Conference. San Diego, USA, 2006: 1154－1159.

[2] Ou S Q, Tu K N. A study of electromigration in Sn-3.5Ag and Sn-3.8Ag-0.7Cu solder lines[C] // Electronic Components and Technology Conference. Lake Buena Vista, 2005: 1445－1450.

[3] Chiang K N, Lee C C, Lee C C. Current crowding-induced electromigration in SnAg3.0Cu0.5 microbumps[J]. Applied Physics Letters, 2006, 88(7): 580－582.

[下转第 42 页]

型内部热流分布所致. 尚需在日后的工作中不断改进.

4 结 论

(1)采用双椭球体热源模式,把过热熔滴带入熔池的热量处理为特定区域内的均匀热源,建立了运动电弧作用下 GMAW 焊接 6 mm低碳钢试件焊接热过程的数值模型.

(2)对 GMAW从起焊到准稳态的焊接熔池形状和表面变形进行了预测,达到宏观准稳态时计算所得的焊缝形状尺寸与试验结果基本吻合.

参考文献:

[1] Wu C S, Dorn L. Prediction of surface depression of a tungsten inert gas weld pool in the full-penetration condition[J]. Journal of Engineering Manufacture, 1995, 209(2): 221-226.

[2] Fan H G, Tsai H L, Na S J. Heat transfer and fluid flow in a partially or fully penetrated weld pool in gas tungsten arc welding[J]. International Journal of Heat and Mass Transfer, 2001, 44(2): 417-428.

[3] Choo R T C, Szekely J, Westhoff R C. Modeling of high-current arcs with emphasis on free surface phenomena in the weld pool[J]. Welding Journal, 1990, 69(9): 346s-361s.

[4] Zhao Ming, Li Ruiying. Numerical analysis of dynamic variation of weld pool geometry in full-penetrated TIG welding[J]. China Welding, 2008, 17(2): 47-53.

作者简介:孙永兴,男,1964年出生,硕士,教授,硕士生导师. 主要研究方向为焊接设备及其自动化、焊接热过程的数值模拟. 发表论文 10余篇.

Email: taiyangyu0631@163.com

[上接第 38页]

[4] Zhang L, Wang Z G, Shang J K. Current-induced weakening of Sn3.5Ag0.7Cu Pb-free solder joints[J]. Scripta Materialia, 2007, 56(5): 381-384.

[5] 董文兴, 郝 虎, 史耀武, 等. 稀土改性的 Sn-58Bi低温无铅钎料[J]. 电子元件与材料, 2007, 26(6): 21-24.
Dong Wenxing, Hao Hu, Shi Yaowu, et al. Rare earth-modified Sn-58Bi low-temperature lead-free solder[J]. Electronic Components and Materials, 2007, 26(6): 21-24.

[6] Miao H W, Duh J G. Microstructure evolution in Sn-Bi and Sn-Bi-Cu solder joints under thermal ageing[J]. Materials Chemistry and Physics, 2001, 71(3): 255-271.

[7] Xu G C, He H W, Guo F. Temperature-dependent phase segregation in Cu/42Sn-58Bi/Cu reaction couples under high current density[J]. Journal of Electronic Materials, 2008, 38(2): 273-283.

[8] He H W, Xu G C, Hao H, et al. Electromigration in lead-free Sn3.8Ag0.7Cu solder reaction couple[C] // 8th International Conference on Electronic Packaging Technology. Shanghai, China, 2007: 225-229.

[9] Chen C M, Huang C C. Atomic migration in eutectic SnBi solder alloys due to current stressing[J]. Journal of Materials Research, 2008, 23(4): 1051-1056.

[10] Chen C M, Chen L T, Lin Y S. Electromigration-induced Bi segregation in eutectic SnBi solder joint[J]. Journal of Electronic Materials, 2007, 36(2): 168-172.

作者简介:何洪文,男,1979年出生,博士. 研究方向为先进电子连接材料及技术. 发表论文 10余篇.

Email: hhw@emails.bjut.edu.cn

(1. School of Material Science and Engineering, Jiangsu University, Zhenjiang 212013, China; 2. State Key Laboratory of Advanced Welding Production Technology, Harbin Institute of Technology, Harbin 150001, China). p17—21

Abstract: The SiC_p/6061Al MMCs joints were produced by arc-ultrasonic plasma arc in-situ weld-alloying by argon-nitrogen mixture as plasma gases and Ti wire as filler composite, and the effect of arc-ultrasonic on the microstructures and mechanical properties of the joints was investigated. The results indicate that without arc-ultrasonic (conventional plasma arc welding (PAW)), new phase AlN is slender needle-like, Al_3Ti is bulky, and the new particles such as TiC and TiN distribute unevenly in weld. Because arc-ultrasonic can refine the new reinforced composites such as TiC and TiN significantly and improve their distribution, new phase Al_3Ti become smaller and less. The test results of mechanical property show that the maximum tensile strength of the welded joint gained with arc-ultrasonic is 225 MPa, raising about 7% compared with conventional PAW.

Key words: SiC_p/Al MMCs; plasma arc welding; arc-ultrasonic; mechanical property

Finite element analysis of residual stress in weld and bolt beam-column connections YU Jiahuan, DAI Li, LIHongshuang, LIU Qiongyang (School of Civil Engineering, Shenyang Jianzhu University, Shenyang 110168, China). p22—26

Abstract: Three dimensional finite element model of welding beam-column connection components including angle steel, bolt, beam and column is established by taking account of the effect of temperature on the thermo-physical properties and mechanical properties of metal, and the temperature and the residual stress distributions during heating and cooling process are accurately computed by using of ANSYS software. The results show that the welding region is dominated mainly by tensile stress and different components possess different residual stress value. The maximum and minimum residual stresses occur in the bolts which are 220.8% and 11.45% of the designing strength value respectively and are in accord with 'Code of Steel Structure'.

Key words: composite connection; welding; bolt; residual stress

Simulation of solidification microstructure in welded molten pool of nickel-based alloy DONG Zhibo[1], MA Rui[1], WANG Yong[2], ZHAN Xiaohong[1], WEI Yanhong[1,3] (1. State Key Laboratory of Advanced Welding Production Technology, Harbin Institute of Technology, Harbin 150001, China; 2. Shanghai Xinli Institute of Power Equipment, Shanghai 200125, China; 3. School of Material Science and Technology, Nanjing University of Aeronautics & Astronautics, Nanjing 210016, China). p27—30

Abstract: Original cellular automaton capture rule was modified and applied to simulate dendrite growth during solidification process in welded molten pool of nickel-based alloy. The results show that the competitive growth between dendrites with different crystallographic axes orientations is intense. The grains whose crystallographic axes orientations are in accordance with the direction of largest temperature gradient have a fast growth speed and overgrow other grains, so that they can keep growing during solidification process. Meanwhile, solute concentrates in the residual liquid in the closed zone among dendrites and dendrite arms, which can lead to severe grain-boundary segregation after solidification process.

Key words: welded molten pool; dendrite growth; epitaxial growth; cellular automaton

Effects of surface state of C/SiC composites on brazing of C/SiC to Nb LIU Yuzhang, ZHANG Lixia, YANG Zhenwen, FENG Jicai, LI Hongwei (State Key Laboratory of Advanced Welding Production Technology, Harbin Institute of Technology, Harbin 150001, China). p31—34

Abstract: C/SiC composites and Nb were brazed with equiatomic ratio Ti-Ni composite foils in vacuum, and the effects of surface state of C/SiC composites on the microstructure and property of the brazing joints were investigated. The results showed that the (Ti, Nb)C reaction layer between C/SiC and filler metal in the brazing joint was serrate when the C/SiC surface state was cut by the electric spark linear cutting machine, but the (Ti, Nb)C layers were both flat when the surface of C/SiC were polished and sanded before brazing. The serrate reaction layer decreased the stress concentration at the C/SiC-filler metal interface and was benefit for the joint. The shear strength of brazing joints of Nb and C/SiC at spark cutting state reached 188 MPa, which is much higher than that at polishing and sanding states. The fracture of brazing joints of Nb and C/SiC at spark cutting state took place at C/SiC base material, C/SiC-filler metal interface and filler metal, but that of the other two kinds of joints mainly occurred at the C/SiC-filler metal interface.

Key words: C/SiC composites; braze; surface state; microstructure; shear strength

Mechanism investigation of Bi layer formation at anode interface in Cu/Sn-58Bi/Cu solder joint induced by electromigration HE Hongwen[1,2], XU Guangchen[1], GUO Fu[1] (1. College of Material Science and Engineering, Beijing University of Technology, Beijing 100124, China; 2. Department of Mechanical Engineering, Tsinghua University, Beijing 100084, China). p35—38, 42

Abstract: Mechanism of Bi layer formation at the anode interface in Cu/Sn-58Bi/Cu solder joint was investigated under current density of 5×10^3 to 1.2×10^4 A/cm^2. During electromigration process, Bi was the main diffusing species which migrated from the cathode side to the anode side under electromigration force. Bi was the first species to reach anode interface because the diffusion velocity of Bi is faster than that of Sn. Therefore, compressive stress was formed at the anode interface when much more Bi atoms accumulated there and compelled Sn to migrate towards the cathode side, and the continuous Bi layer was formed at the anode interface. In the mean time, tensile stress was formed at the cathode interface due to the departure of metal atoms, which led to voids and cracks formation. The morphology of the Bi layer included planar-type layer and groove-type layer. The diffusing channels of the Bi atoms were Bi grain boundaries, Sn grain boundaries and Sn/Bi interfaces. With the current density and stressing time increasing, the Bi layer thickness increased. The electromigration force and Joule heating took on the

main driving force for Bi diffusion and migration.

Key words: electromigration; Bi layer; current density; Joule heating

Numerical simulation of weld pool geometry and surfaces deformation in GMAW

SUN Yongxing, ZHAI Lei, ZHAO Ming (1. College of Mechanical & Electronic Engineering, China University of Petroleum, Dongying 257061, China; 2. Shengli Engineering & Consulting Co., Ltd., Dongying 257026, China). p. 39—42

Abstract: Numerical simulation analysis model for gas metal arc welding (GMAW) was created in the course of the welding heat based on Visual Fortran. A double ellipsoid heat source mode was adopted to depict the distribution of a moving GMAW arc. Transient variations of weld pool geometry and free surfaces deformation were predicted and verified. The results show that the calculated width and depth of molten pool are in agreement with those of the experimental results.

Key words: gas metal arc welding; free surfaces deformation; double ellipsoid heat source; numerical analysis

Microstructure and properties of WC-4Co ESD coating of cast steel roll

WANG Jiansheng, MENG Huimin, ZHANG Ruizhu, YAN Dakao (1. North China Institute of Water Conservancy and Hydroelectric Power, Zhengzhou 450011, China; 2. College of Materials Science and Engineering, University of Science and Technology Beijing, Beijing 100083, China). p. 43—46

Abstract: WC-4Co electrode material is deposited on the surface of cast steel roll by electro-spark deposition (ESD). The microstructure and wear resistance of the coating are investigated. The results show that the coating consists of Fe_3W_3C, Co_3W_3C, Fe and SiC phases, and the coating bonded with cast steel roll substrate is well metallurgical. The phases of Fe_3W_3C and Co_3W_3C distribute dispersedly in the coating with the extra-fine structure. The average hardness of the coating is 1 617.2 HV. The resistance performance of the coating is 2.1 times higher than that of the cast steel substrate. The wear mechanism is adhesion wear, fatigue wear, oxidization wear and abrasive wear, but the main wear mechanism is fatigue wear and abrasive wear.

Key words: electro-spark deposition; WC-4Co; cast steel roll; microstructure; wear resistance

Analysis of microstructure and properties of Ti-C-WC reinforced Ni-based composite coating by argon arc cladding

WANG Yongdong, WANG Zhenting, ZHANG Haijun, ZHU Yan (Department of Material Science and Technology, Heilongjiang Institute of Science and Technology, Harbin 150022, China). p. 47—49

Abstract: Ni-based composite coating reinforced with the pre-alloyed powder of Ni60A, WC, Ti and C was prepared on the surface of Q235 steel by means of argon arc cladding technique. The microstructure was investigated by using optical microscope, scanning electron microscope and X-ray diffraction. The results show that the main phases of coating are TiC, (Ti, W)C, γ-Ni dendrite structure and $M_{23}C_6$ eutectic structure. The grain of TiC is fine, which size is about 1.5 μm, and distributes uniformly. The test results of micro-hardness and wear resistance show that the micro-hardness is improved about 4 times compared with that of the Q235 steel. The argon arc cladding composite coating has high hardness and excellent wear resistance under dry sliding wear test conditions.

Key words: argon arc cladding; composite coating; micro-hardness; wear resistance

Ultrasonic pulse tungsten inert-gas arc welding of Ti-6Al-4V alloy

ZHOU Shuiliang, ZHAO Haitao, QI Bojin (1. Aeronautical Key Laboratory for Aviation Joining Technology, Beijing Aeronautical Manufacturing Technology Research Institute, Beijing 100024, China; 2. School of Mechanical Engineering and Automation, Beijing University of Aeronautics & Astronautics, Beijing 100191, China). p. 50—52

Abstract: Ti-6Al-4V alloy was welded by conventional tungsten inert-gas arc welding (TIG) and ultrasonic pulse TIG welding (U-TIG) respectively. The microstructure of the joint was analyzed by means of optical microscope, scanning electron microscope and X-ray diffraction to study the relationship between the macro-properties and the microstructure of the joint. The results show that U-TIG welding can reduce pores of joint. With the increment of pulse frequency, the microstructure becomes finer and finer and is inclined to equiaxed crystal, while pulse frequency is 45 kHz, the effect of grain refinement is the best. Moreover, the properties of joint by U-TIG welding are improved compared with that of conventional TIG. The tensile fractures of the joints welded by TIG and U-TIG all present the character of quasi-cleavage crack, but the cellular dendrite depredation is not observed obviously in U-TIG joint.

Key words: ultrasonic pulse TIG welding; conventional TIG welding; Ti-6Al-4V titanium alloy

Optimization design of twin-wire welding temperature field algorithm procedures

YANG Xiuzhi, YU Shengfu, YAO Rungang (1. Materials College, Huazhong University of Science and Technology, Wuhan 430070, China; 2. Materials Institute 725 of Luoyang Ship, Luoyang, 471039, China). p. 53—56

Abstract: The temperature field of the twin-wire submerged arc welding was analyzed by finite element software ANSYS of secondary development. The calculation and loading of heat of mobile heat source were programmed by ANSYS parametric design language. In particular, by the use of vector, the calculation and loading operation were simplified and the efficiency of simulation was improved. The experiments verify that the algorithm of heat load makes simulation time and calculation reduce, and the algorithm is feasible and efficient. This algorithm can be applied to the thermal calculation and loading of temperature field for multiple wire welding.

Key words: twin-wire submerged arc welding; mobile source; algorithm; vector

Effect of Mn content on CGHAZ microstructure and properties of large heat input welding in ship steels

LUO Xiaobing, SU Hang, YANG Caifu, CHAI Feng, YUAN Xiaomin (1. School of Materials Science and Engineering, Anhui University of Technology, Maanshan 243002, China; 2. Institu-